Int. J. of Heat and Fluid Flow, Vol. 86, No. 108666, 2020, doi.org/10.1016/j.ijheatfluidflow.2020.108666

A formulation of PANS capable of mimicking IDDES

Christophe Friess

M2P2 UMR 7340, Aix-Marseille Université, CNRS, Centrale Marseille, 13451, Marseille, France, christophe.friess@univ-amu.fr

Lars Davidson

Division of fluid dynamics, Department of Mechanics and Maritime Sciences, Chalmers University of Technology, SE-412 96 Gothenburg, Sweden, lada@chalmers.se

Abstract

The partially averaged Navier-Stokes (PANS) model, proposed in [1], allows to simulate turbulent flows either in RANS, LES or DNS mode. The PANS model includes f_k which denotes the ratio of modeled to total kinetic energy. In RANS, $f_k = 1$ while in DNS it tends to zero. In the present study we propose an improved formulation for f_k based on the H-equivalence introduced by Friess *et al.* (2015). In this formulation the expression of f_k is derived to mimic Improved Delayed Detached Eddy Simulation (IDDES). This new formulation behaves in a very similar way as IDDES, even though the two formulations use different mechanisms to separate modeled and resolved scales. They show very similar performance in separated flows as well as in attached boundary layers. In particular, the novel formulation is able to (i) treat attached boundary layers as properly as IDDES, and (ii) "detect" laminar initial/boundary conditions, in which case it enforces RANS mode. Furthermore, it is found that the new formulation is numerically more stable than IDDES.

Keywords: LES; PANS; IDDES; channel flow; hill flow; hump flow

1. Introduction

The Partially Averaged Navier-Stokes (PANS) approach was originally proposed by Girimaji [1], based on the scale separation between resolved and unresolved parts of the turbulent fluid motion, making use of the parameter f_k, which represents the modeled-to-total turbulent kinetic energy ratio. The way of prescribing f_k has been subject of a huge research effort. Recently, Klapwijk *et al.* [2] made a comparative review of differents ways of prescribing f_k, distinguishing two categories: static and dynamic formulations. Almost simultaneously with PANS, Partially Integrated Transport Model (PITM, see e.g. [3, 4]), was derived from multiscale approaches in spectral space, but also using the modeled-to-total turbulent kinetic energy ratio f_k.

Detached Eddy Simulation was developed almost a decade earlier, based on rather empirical fundaments, by Spalart *et al.* [5]. Their approach turned out to be very efficient in predicting unsteady features of flows out of equilibrium, but less so in flows involving thick boundary layers or shallow separations. A first improvement of DES was Delayed Detached Eddy Simulation (DDES) [6], able to overcome the aforementioned issues. More recently, the DES community formulated Improved Delayed Detached Eddy Simulation (IDDES) [7], designed to act as a proper (i) wall-modeling approach for LES and (ii) RANS model when no turbulent content is provided in initial/boundary conditions.

Friess *et al.* [8] established an equivalence criterion between DES and other seamless hybrid RANS/LES approaches like PANS and PITM and formulated a postulate of equivalence: *"Two hybrid approaches based on the same closure, but using a different method of control of the energy partition, yield similar low-order statistics of the resolved velocity fields provided that they yield the same level of subfilter energy."*. A by-product of that work is a new hybrid method, taking the shape of a DES designed with the energy ratio f_k instead of the explicit grid step Δ. Later, Davidson & Friess [9] used this result the other way around, proposing a way to prescribe f_k in PANS (as well as in PITM) derived from the so-called "DES97" methodology. The model is denoted D-PANS. This

formulation showed several interesting features (behaviour very similar to that of actual DES, self-adaptivity, better performance than PANS with fixed f_k ...) The present project aims at developing an improved formulation for f_k, gathering the interesting features of IDDES enumerated above, and the strong theoretical background of PANS.

The paper is organized as follows. First, the rationale of PANS, IDDES and the derivation of their equivalence criterion, is presented in Sec. 2. This derivation leads to a new approach, that will be called IDD-PANS. The solver used for the computations is presented in Sec. 3. In Sec. 4, IDDES and IDD-PANS, along with the D-PANS approach, are compared in three different flows (channel flow, hump flow and hill flow). Some conclusions are drawn in the final section.

2. Rationale

In this section, the PANS and IDDES models are presented. They use different cutoff functions, to perform the separation between resolved and unresolved scales. Note that the unresolved scales correspond to the subgrid scales in LES mode, and to the modeled scales in RANS.

- PANS controls the destruction of unresolved dissipation, through the adaptive coefficient $C^*_{\varepsilon 2}$. Moreover, in PANS, diffusion coefficients are also tuned according to the cutoff. The idea is to damp modeled turbulent kinetic energy as the resolution gets finer.

- Though using the same idea of damping the modeled turbulent kinetic energy as above, DES and IDDES act in a more direct way. The sink term entering the unresolved turbulent kinetic energy equation is multiplied by an adaptive coefficient ψ.

Details are given below.

2.1. The PANS model

The low-Reynolds number Partially-Averaged Navier-Stokes (LRN PANS, see [10]) uses the AKN $k-\varepsilon$ turbulence model [11] as parent RANS and reads

$$\begin{aligned}
\frac{Dk_u}{Dt} &= \frac{\partial}{\partial x_j}\left[\left(\nu+\frac{\nu_{tu}}{\sigma_{ku}}\right)\frac{\partial k_u}{\partial x_j}\right]+P_{ku}-\varepsilon_u \\
\frac{D\varepsilon_u}{Dt} &= \frac{\partial}{\partial x_j}\left[\left(\nu+\frac{\nu_{tu}}{\sigma_{\varepsilon u}}\right)\frac{\partial \varepsilon_u}{\partial x_j}\right]+C_{\varepsilon 1}P_{ku}\frac{\varepsilon_u}{k_u}-C^*_{\varepsilon 2}\frac{{\varepsilon_u}^2}{k_u} \\
\nu_{tu} &= C_\mu f_\mu \frac{{k_u}^2}{\varepsilon_u}, P_{ku}=2\nu_{tu}\bar{s}_{ij}\bar{s}_{ij}, \bar{s}_{ij}=\frac{1}{2}\left(\frac{\partial \bar{v}_i}{\partial x_j}+\frac{\partial \bar{v}_j}{\partial x_i}\right) \\
C^*_{\varepsilon 2} &= C_{\varepsilon 1}+\frac{f_k}{f_\varepsilon}(C_{\varepsilon 2}f_2-C_{\varepsilon 1}), \sigma_{ku}\equiv\sigma_k\frac{f_k^2}{f_\varepsilon}, \sigma_{\varepsilon u}\equiv\sigma_\varepsilon\frac{f_k^2}{f_\varepsilon} \\
\sigma_k &= 1.4, \sigma_\varepsilon = 1.4, C_{\varepsilon 1}=1.5, C_{\varepsilon 2}=1.9, C_\mu = 0.09
\end{aligned} \tag{1}$$

where $D/Dt=\partial/\partial t+\bar{v}_j\partial/\partial x_j$ denotes the material derivative. The damping functions are given by

$$\begin{aligned}
f_2 &= \left[1-\exp\Big(-\frac{y^*}{3.1}\Big)\right]^2\left\{1-0.3\exp\left[-\Big(\frac{R_{tu}}{6.5}\Big)^2\right]\right\} \\
f_\mu &= \left[1-\exp\Big(-\frac{y^*}{14}\Big)\right]^2\left\{1+\frac{5}{R_{tu}^{3/4}}\exp\left[-\Big(\frac{R_{tu}}{200}\Big)^2\right]\right\}
\end{aligned}$$

$$R_{tu}=\frac{{k_u}^2}{\nu\varepsilon_u}, \quad y^*=\frac{U_\varepsilon y}{\nu}, \quad U_\varepsilon=(\varepsilon_u\nu)^{1/4} \tag{2}$$

The subscript u refers to the unresolved motion. The functions f_k and f_ε denote the ratio of modeled to total kinetic energy and modeled to total dissipation, respectively. For flows at high Reynolds numbers (as in the present work), the dissipation is modeled which means that $f_\varepsilon = 1$. In the PITM model, $\sigma_{ku}\equiv\sigma_k$ and $\sigma_{\varepsilon u}\equiv\sigma_\varepsilon$. Note that, in PANS, $C^*_{\varepsilon 2}$ is the control parameter for the resolution, with $\psi = 1$ (its RANS value).

2.2. The IDDES model

The aforementioned LRN model can be transposed to an IDDES form, also based on the AKN $k-\varepsilon$ turbulence model as parent RANS:

$$\begin{aligned}
\frac{Dk_u}{Dt} &= \frac{\partial}{\partial x_j}\left[\left(\nu+\frac{\nu_{tu}}{\sigma_{ku}}\right)\frac{\partial k_u}{\partial x_j}\right] + P_{ku} - \psi\varepsilon_u \\
\frac{D\varepsilon_u}{Dt} &= \frac{\partial}{\partial x_j}\left[\left(\nu+\frac{\nu_{tu}}{\sigma_{\varepsilon u}}\right)\frac{\partial \varepsilon_u}{\partial x_j}\right] + C_{\varepsilon 1}P_{ku}\frac{\varepsilon_u}{k_u} - C_{\varepsilon 2}f_2\frac{{\varepsilon_u}^2}{k_u} \\
\nu_{tu} &= C_\mu f_\mu \frac{{k_u}^2}{\varepsilon_u}, P_{ku} = 2\nu_{tu}\bar{s}_{ij}\bar{s}_{ij}, \bar{s}_{ij} = \frac{1}{2}\left(\frac{\partial \bar{v}_i}{\partial x_j}+\frac{\partial \bar{v}_j}{\partial x_i}\right) \\
\sigma_k &= 1.4, \sigma_\varepsilon = 1.4, C_{\varepsilon 1} = 1.5, C_{\varepsilon 2} = 1.9, C_\mu = 0.09
\end{aligned} \tag{3}$$

The damping functions are the same as in the LRN PANS model (given by Eq. (2)).

Note that, in (ID)DES, ψ is the control parameter for the resolution, while $C_{\varepsilon 2}$ is set to its RANS value. The function ψ may be more or less sophisticated. In all cases, we write ψ as:

$$\psi = \frac{l_u}{\tilde{l}} \ . \tag{4}$$

Let us define three length scales:

- l_u, the characteristic (local and instantaneous) length scale of the unresolved scales,
- l_c, the characteristic length scale of the cutoff,
- $\tilde{l}$, the reference length scale.

Those length scales read

$$l_u = \frac{k_u^{3/2}}{\varepsilon_u} \ , \tag{5}$$

and

$$l_c = C_{DES}\Delta \ . \tag{6}$$

The key difference between DES and IDDES lies in the prescription of $\tilde{l}$ entering Eq. (4). In original DES, the reference length scale $\tilde{l}$ simply reads:

$$\tilde{l} = \min\left(l_u; l_c\right) \ . \tag{7}$$

In IDDES, it is more sophisticated. The grid step Δ is also chosen in a more complex way. These differences are discussed below.

2.2.1. Cut-off length scale

The cut-off length scales is defined as:

$$l_c = \Psi C_{DES} \Delta \ , \tag{8}$$

where Ψ is a low-Reynolds number correction (see Eq. 10), and Δ:

- the maximum grid step h_{max} in DES,
- a *corrected* grid step, designed to improve the WMLES (wall-modeled LES) capabilities of DES. It reads:

$$\Delta = \min\left\{\max\left[C_w d_w; C_w h_{max}; h_{wn}\right]; h_{max}\right\} \ , \tag{9}$$

  where

  - $C_w = 0.15$ is a constant, presumably independent of the turbulent closure,
  - d_w is the distance to the closest wall,
  - h_{wn} is the grid step in the wall normal direction.

The low-Reynolds correction Ψ (see e.g. [7, 6]) depends on the turbulent closure, and is set so that at equilibrium (neither convection nor diffusion in the closure equations), the eddy viscosity obeys a Smagorinsky-like law, in LES mode. This correction is only needed for closure models using some low-Reynolds features, which is the case of the model used here, and summarized in Eq. (1), and Ψ reads:

$$\Psi = \min\left\{10; \left(f_2 f_\mu\right)^{-3/4}\right\} \tag{10}$$

where f_2 and f_μ are given by Eq. 2.1 and the limiting value of 10 is added to ensure reasonable behavior of Ψ in the "DNS limit", i.e. $\nu_{t_u} < \nu/100$, as prescribed in [6]. Details on the calibration of Ψ are given in Appendix A.

2.2.2. Reference length scale

In contrast with its formulation given by Eq. (7) in DES, the reference length scale $\tilde{l}$ is, in IDDES, a blending between l_u and l_c. It reads:

$$\tilde{l} = \tilde{f}_d \left(1 + f_e\right) l_u + \left(1 - \tilde{f}_d\right) l_c \ , \tag{11}$$

where l_u is defined by (5) and l_c by (8). The blending functions $\tilde{f}_d$ and f_e read:

$$\tilde{f}_d = \max\left\{(1 - f_{dt})\,; f_B\right\} \ , \tag{12}$$

$$f_e = \max\left\{(f_{e1} - 1)\,; 0\right\}\Psi f_{e2} \ , \tag{13}$$

where Ψ is given by Eq. (10) and the functions f_{dt} and f_B entering Eq. (12) are given by:

$$f_{dt} = 1 - \tanh\left[(8r_{dt})^3\right] \ , \tag{14}$$

$$f_B = \min\left\{2\exp\left(-9\alpha^2\right); 1\right\} \ , \tag{15}$$

with

$$\alpha = 0.25 - d_w/h_{max} \ . \tag{16}$$

The functions f_{e1} and f_{e2} in Eq. (13) read:

$$f_{e1} = \begin{cases} 2\exp\left(-11.09\alpha^2\right) & \text{if } \alpha \geq 0 \\ 2\exp\left(-9\alpha^2\right) & \text{if } \alpha < 0 \end{cases} \ , \tag{17}$$

and

$$f_{e2} = 1 - \max\left\{f_t; f_l\right\} \ , \tag{18}$$

where the functions f_t and f_l are given by:

$$f_t = \tanh\left[\left(c_t^2 r_{dt}\right)^3\right] \ , \tag{19}$$

$$f_l = \tanh\left[\left(c_l^2 r_{dl}\right)^{10}\right] \ . \tag{20}$$

The constants c_t and c_l above, depend on the background RANS model. They were originally tuned in [7] for the SA model, and later in [12] for the $k-\omega$ SST model. The chosen values are $c_t = 1.87$ and $c_l = 5$.

The quantities r_{dt} (also entering Eq. 14) and r_{dl}, are defined as follows:

$$r_{dt} = \frac{\nu_t}{\kappa^2 d_w^2 \max\left\{\mathcal{S}; 10^{-10}\right\}} \ , \tag{21}$$

$$r_{dl} = \frac{\nu}{\kappa^2 d_w^2 \max\left\{\mathcal{S}; 10^{-10}\right\}} \ , \tag{22}$$

where

$$\mathcal{S} = \sqrt{\sum_{ij}\left(\frac{\partial u_i}{\partial x_j}\right)^2} \ . \tag{23}$$

In what follows, we derive a relationship between the cutoff control functions ψ of IDDES and f_k (or equivalently, $C^*_{\varepsilon 2}$) of PANS.

2.3. Equivalence between PANS and DES/IDDES

Friess *et al.* [8] made a first attempt in bridging DES and PITM. They derived equivalence criteria in three major cases:

- homogeneous equilibrium layers,
- inhomogeneous flows,
- allowing filter-induced modifications of the unresolved dissipation rate (while the two previous cases assume that it is not affected by the energy partition).

In that aim, they considered infinitesimal perturbations in the equilibrium of the ensemble-averaged $k_u - \varepsilon_u$ system, when introducing $\delta\psi$ for DES and $\delta C^*_{\varepsilon 2}$ for PITM, given that in RANS mode, $\psi = f_k = 1$ and $C^*_{\varepsilon 2} = C_{\varepsilon 2}$. Then, integrating the result between RANS and an arbitrary state, yields a relationship evaluating ψ for a given f_k.

More recently, Davidson & Friess [9] used the aforementioned relationship in a reverse way, in order to obtain some new way to define the f_k factor for PANS, ψ being given by DES (see Eqs. (5)-(7) in the present paper). However, their work was a first attempt, as (i) they just considered the homogeneous equilibrium layer case in their derivation and (ii) they restricted their study to DES. In [13], they showed that this method works pretty much like DES.

Now, in the present work, we consider inhomogeneous flows, which are more relevant in engineering. Let us define k_M and ε_M such as:

$$k_M = \langle k_u \rangle \tag{24}$$

$$\varepsilon_M = \langle \varepsilon_u \rangle \tag{25}$$

where $\langle . \rangle$ denotes the ensemble average. Along mean streamlines, k_M and ε_M are assumed to be in equilibrium, which yields, when describing both PANS and

(ID)DES:

$$\frac{Dk_M}{Dt} = P^k + D^k - \psi\varepsilon_M = 0 \tag{26}$$

$$\frac{D\varepsilon_M}{Dt} = C_{\varepsilon 1}\frac{\varepsilon_M}{k_M}P^k + D^\varepsilon - C^*_{\varepsilon 2}\frac{\varepsilon_M^2}{k_M} = 0 \tag{27}$$

where P^k denotes the production of k_M and D^k and D^ε the diffusion terms of k_M and ε_M respectively.

In order to perform the perturbation analysis, some assumptions are needed. First, since in Sec. 2.1, we assumed that $f_\varepsilon = 1$, it yields:

$$\delta\varepsilon_M = 0 \tag{28}$$

Following [8], we add the heuristic assumption that the relative variation $\delta k_M/k_M$ does not vary in space, which allows to state:

$$\frac{\partial\left(k_M + \delta k_M\right)}{\partial x_j} = \left(1 + \frac{\delta k_M}{k_M}\right)\frac{\partial k_M}{\partial x_j} \tag{29}$$

$$\frac{\partial^2\left(k_M + \delta k_M\right)}{\partial x_j \partial x_j} = \left(1 + \frac{\delta k_M}{k_M}\right)\frac{\partial^2 k_M}{\partial x_j \partial x_j} \tag{30}$$

Furthermore, by definition,

$$f_k = k_M/k_{tot} \tag{31}$$

where k_{tot} is the total (resolved + modeled) turbulent kinetic energy.

2.3.1. PANS equations

For the PANS method (ψ=1), the equations for infinitesimal perturbations of Eqs (26)-(27) are:

$$\delta P^k + \delta D^k = 0 \tag{32}$$

$$C_{\varepsilon 1}\frac{\varepsilon_M}{k_M}P^k\left(\frac{\delta P^k}{P^k} - \frac{\delta k_M}{k_M}\right) - C^*_{\varepsilon 2}\frac{\varepsilon_M^2}{k_M}\left(\frac{\delta C^*_{\varepsilon 2}}{C^*_{\varepsilon 2}} - \frac{\delta k_M}{k_M}\right) + \delta D^\varepsilon = 0 \tag{33}$$

At sufficiently high Reynolds number, the diffusion terms D^k and D^ε can be written:

$$D^k = \frac{\partial}{\partial x_j}\left[\frac{C}{\sigma_k f_k^2}\frac{k_M^2}{\varepsilon_M}\frac{\partial k_M}{\partial x_j}\right] \tag{34}$$

$$D^\varepsilon = \frac{\partial}{\partial x_j}\left[\frac{C}{\sigma_\varepsilon f_k^2}\frac{k_M^2}{\varepsilon_M}\frac{\partial \varepsilon_M}{\partial x_j}\right] \tag{35}$$

Using Eqs. (28)-(31) to differentiate Eqs. (34) and (35), it can be shown that:

$$\frac{\delta D^k}{D^k} = \frac{\delta k_M}{k_M} \tag{36}$$

$$\frac{\delta D^\varepsilon}{D^\varepsilon} = 0 \tag{37}$$

Thus, the following relation is obtained:

$$\delta C^*_{\varepsilon 2} = \left(C^*_{\varepsilon 2} - C_{\varepsilon 1}\right) \frac{\delta k_M}{k_M} \tag{38}$$

2.3.2. (ID)DES equations

The same procedure is done with the (ID)DES system ($C^*_{\varepsilon 2} = C_{\varepsilon 2}$). The equations for infinitesimal perturbations of Eqs (26)-(27) are:

$$\delta P^k + \delta D^k + \varepsilon_M \delta\psi = 0 \tag{39}$$

$$C_{\varepsilon 1}\frac{\varepsilon_M}{k_M} P^k \left(\frac{\delta P^k}{P^k} - \frac{\delta k_M}{k_M}\right) + C_{\varepsilon 2}\frac{\varepsilon_M^2}{k_M}\left(\frac{\delta k_M}{k_M}\right) + \delta D^\varepsilon = 0 \tag{40}$$

At sufficiently high Reynolds number, the diffusion terms D^k and D^ε can be written:

$$D^k = \frac{\partial}{\partial x_j}\left[\frac{C}{\sigma_k}\frac{k_M^2}{\varepsilon_M}\frac{\partial k_M}{\partial x_j}\right] \tag{41}$$

$$D^\varepsilon = \frac{\partial}{\partial x_j}\left[\frac{C}{\sigma_\varepsilon}\frac{k_M^2}{\varepsilon_M}\frac{\partial \varepsilon_M}{\partial x_j}\right] \tag{42}$$

Note that, contrary to PANS, there is no f_k correction in the diffusivity. Like for PANS above, we use Eqs. (28)-(31) to differentiate Eqs. (41) and (42). As a result, it can be shown that

$$\frac{\delta D^k}{D^k} = 3\frac{\delta k_M}{k_M} \tag{43}$$

$$\frac{\delta D^\varepsilon}{D^\varepsilon} = 2\frac{\delta k_M}{k_M} \tag{44}$$

As a result, the following relation is obtained:

$$\delta\psi = 3\frac{\left(C_{\varepsilon 1}\psi - C_{\varepsilon 2}\right)}{C_{\varepsilon 1}}\frac{\delta k_M}{k_M} \tag{45}$$

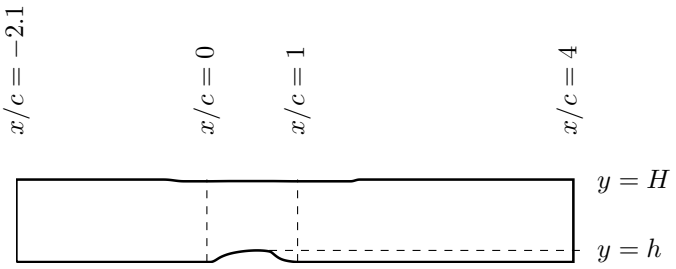

Figure 1: The geometry of the hump.

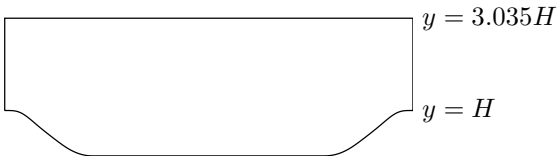

Figure 2: The geometry of the hill.

Now, equalizing $\delta k_M/k_M$ in Eqs. (38) and (45) and integrating the obtained relation between RANS ($C^*_{\varepsilon 2} = C_{\varepsilon 2}$ and $\psi = 1$) and an arbitrary state, yields:

$$\begin{aligned} \int_{C_{\varepsilon 2}}^{C^*_{\varepsilon 2}} \frac{x}{x - C_{\varepsilon 1}} &= \int_1^{\psi} -\frac{C_{\varepsilon 1} dy}{3C_{\varepsilon 1} y - C_{\varepsilon 2}} \Rightarrow \\ \ln\left(\frac{C^*_{\varepsilon 2} - 1}{C_{\varepsilon 2} - 1}\right) &= \frac{1}{3} \ln\left(\frac{C_{\varepsilon 1}\psi - C_{\varepsilon 2}}{C_{\varepsilon 2} - C_{\varepsilon 1}}\right) \end{aligned} \tag{46}$$

As a consequence, when ensuring that $0 \leq f_k \leq 1$ we get

$$f_k = \min\left[1, \max\left(0, \left(\frac{C_{\varepsilon 2} - C_{\varepsilon 1}\psi}{C_{\varepsilon 2} - C_{\varepsilon 1}}\right)^{1/3}\right)\right] \tag{47}$$

It is worth mentioning that the relationship (47) was derived without assuming the way of defining ψ, i.e. regardless of whether ψ is defined in a DES or an IDDES way. However, since we aim at building a formulation of PANS that is equivalent to IDDES, we will consider the latter, (i.e. ψ is defined through Eqs. (4), (5), (8) and (11)).

3. Numerical solver

An incompressible, finite volume code is used [18]. The convective terms in the momentum equations are discretized using central differencing. Hybrid

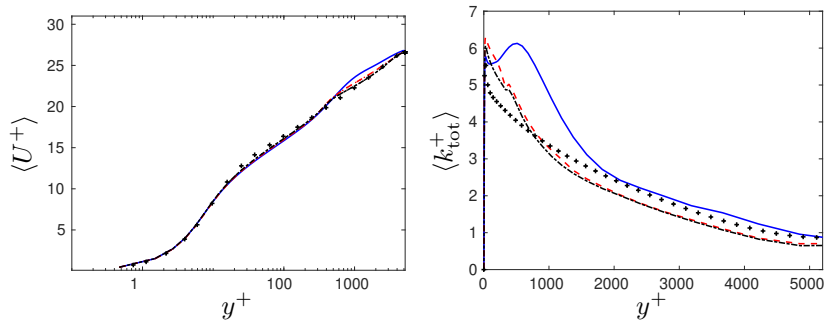

(a) Velocity

(b) Total turbulent kinetic energy

(c) Total turbulent shear stress

(d) Ratio between production and dissipation rate of k_{tot}

Figure 3: Channel flow, $Re_\tau = 5\,200$. ——: D-PANS; – – –: IDD-PANS; – · –: IDDES; Markers: DNS [14]

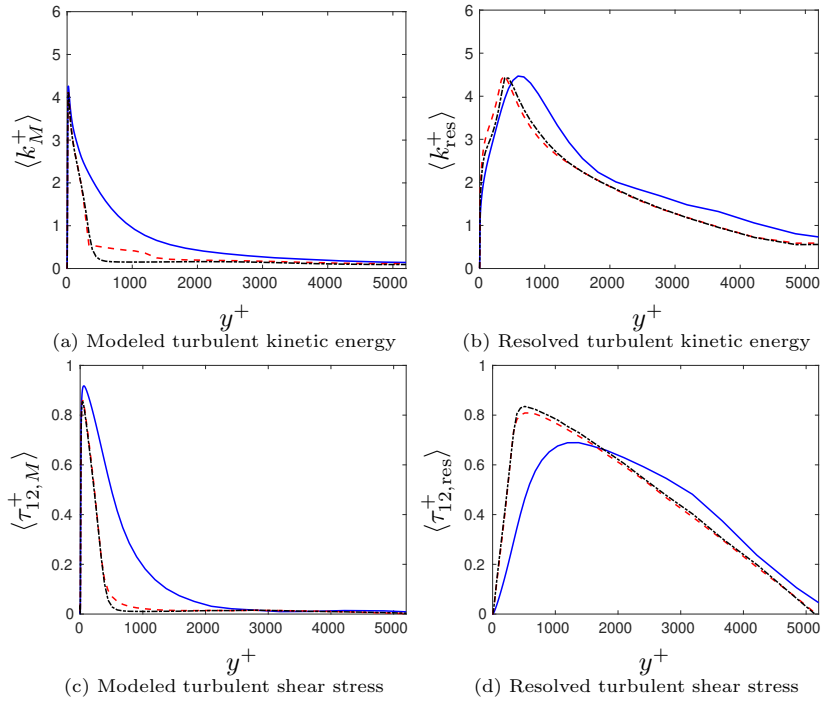

(a) Modeled turbulent kinetic energy

(b) Resolved turbulent kinetic energy

(c) Modeled turbulent shear stress

(d) Resolved turbulent shear stress

Figure 4: Channel flow, $Re_\tau = 5\,200$. —— : D-PANS; – – : IDD-PANS; –·– : IDDES; Markers: DNS [14]

central/upwind is used for the k_u and ε_u equations. The Crank-Nicolson scheme is used for time discretization of all equations. The numerical procedure is based on an implicit, fractional step technique with a multigrid pressure Poisson solver [19] and a non-staggered grid arrangement.

The filtered momentum equations with an added turbulent viscosity ν_{tu} to account for the effect of the unresolved scales on the resolved motion, read

$$\frac{\partial \bar{v}_i}{\partial t} + \frac{\partial \bar{v}_j \bar{v}_i}{\partial x_j} = \beta \delta_{1i} - \frac{1}{\rho}\frac{\partial \bar{p}}{\partial x_i} + \frac{\partial}{\partial x_j}\left((\nu + \nu_{tu}) \frac{\partial \bar{v}_i}{\partial x_j} \right) \tag{48}$$

where the first term on the right side is the driving pressure gradient in the streamwise direction, which is used in the fully-developed channel flow simulations and for the hill flow.

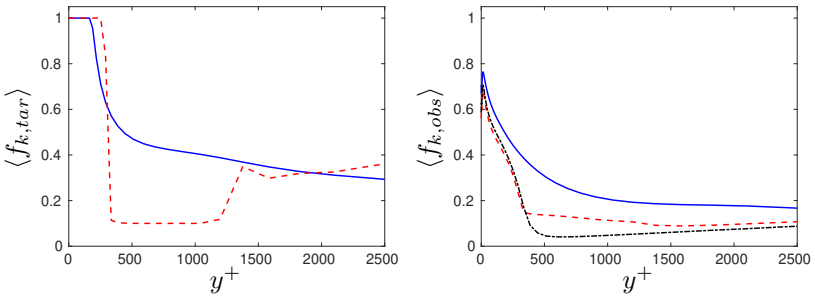

(a) Target f_k. (b) Observed f_k.

Figure 5: Channel flow. f_k. $Re_\tau = 5\,200$. ——: D-PANS; – –: IDD-PANS; –·–: IDDES.

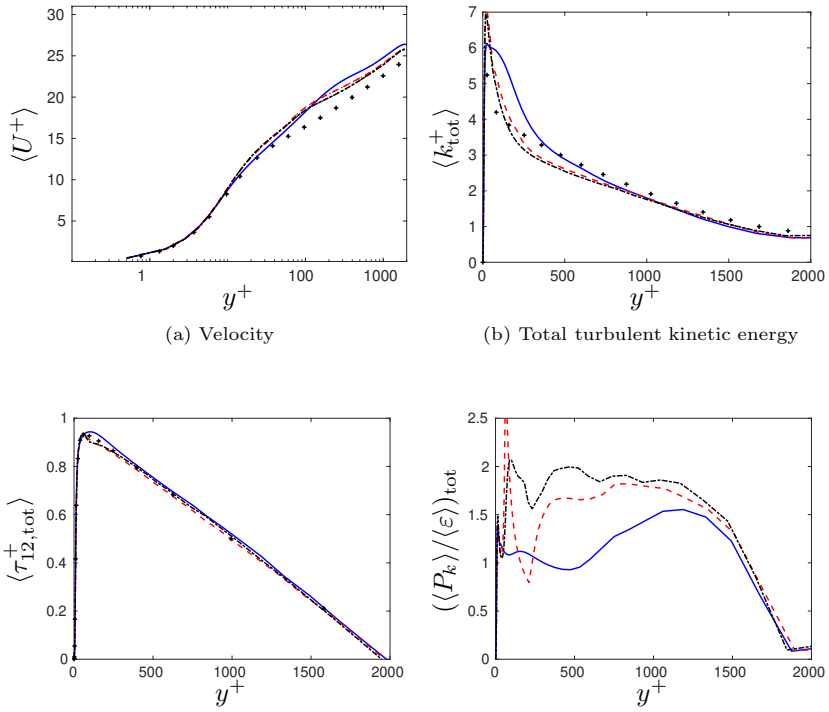

(a) Velocity (b) Total turbulent kinetic energy

(c) Total turbulent shear stress (d) Ratio between production and dissipation of k_{tot}

Figure 6: Channel flow, $Re_\tau = 2\,000$. ——: D-PANS; – –: IDD-PANS; –·–: IDDES; Markers: DNS [14]

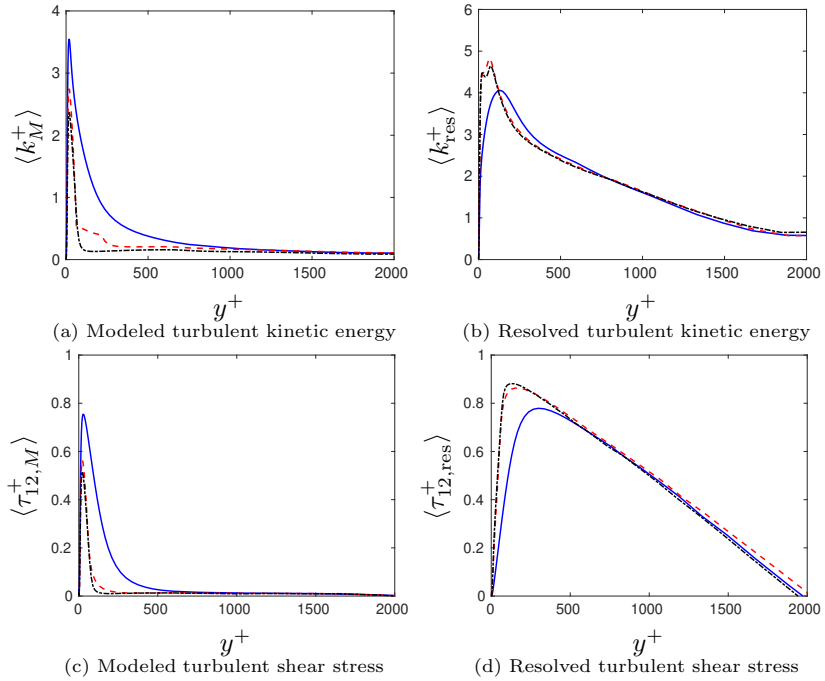

(a) Modeled turbulent kinetic energy

(b) Resolved turbulent kinetic energy

(c) Modeled turbulent shear stress

(d) Resolved turbulent shear stress

Figure 7: Channel flow, $Re_\tau = 2\,000$. ——: D-PANS; – –: IDD-PANS; –·–: IDDES; Markers: DNS [14]

4. Results

In order to validate the IDDES capabilities of the approach developed in Sec. 2, denoted *IDD-PANS*, we will now perform a comparison of IDD-PANS with actual IDDES, using the same turbulent closure model (AKN). In IDDES, we compute ψ and its related coefficients using Eqs. (4) to (23). In IDD-PANS, the same ψ is used to prescribe $f_{k,tar}$ following Eq. (47) . For the sake of performance comparison, results obtained with the D-PANS approach (also using the AKN closure model) are shown as well. It is worth recalling that there is a distinction to make between $f_{k,obs}$, the *observed* energy ratio defined as:

$$f_{k,obs} = \frac{k_M}{k_{tot}} \tag{49}$$

and $f_{k,tar}$, the *targeted* (or prescribed) energy ratio. In IDD-PANS $f_{k,tar} = f_k$ (computed in Eq. 47) is used, but there is usually a discrepancy between $f_{k,obs}$

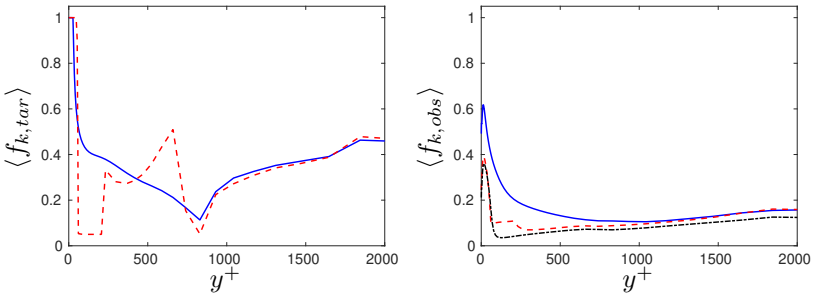

(a) Target f_k. (b) Observed f_k.

Figure 8: Channel flow. f_k. $Re_\tau = 2\,000$. : D-PANS; : IDD-PANS; : IDDES.

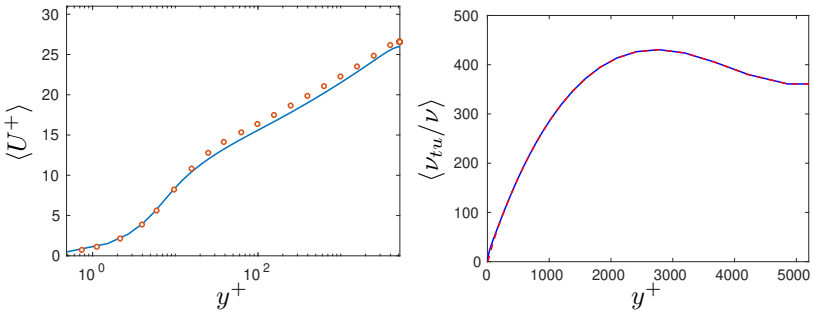

(a) Velocity. (b) Unresolved turbulent viscosity.

Figure 9: Channel flow with steady initial conditions. $Re_\tau = 5\,200$. : IDD-PANS; : 1D AKN RANS; Markers: DNS [14]

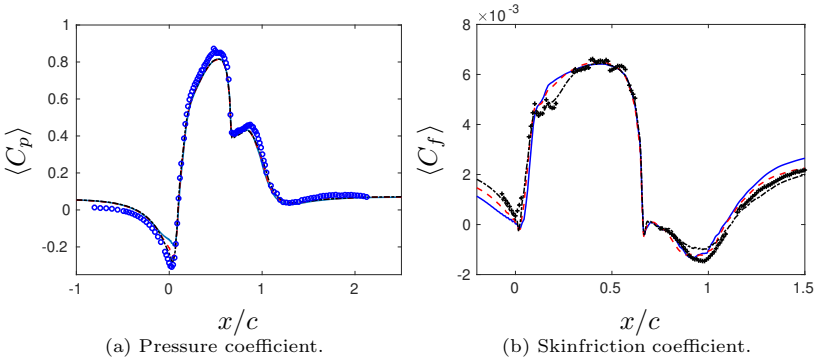

(a) Pressure coefficient. (b) Skinfriction coefficient.

Figure 10: Hump flow. Pressure coefficient and skinfriction. : D-PANS; : IDD-PANS; : IDDES; markers: Experiments [15, 16].

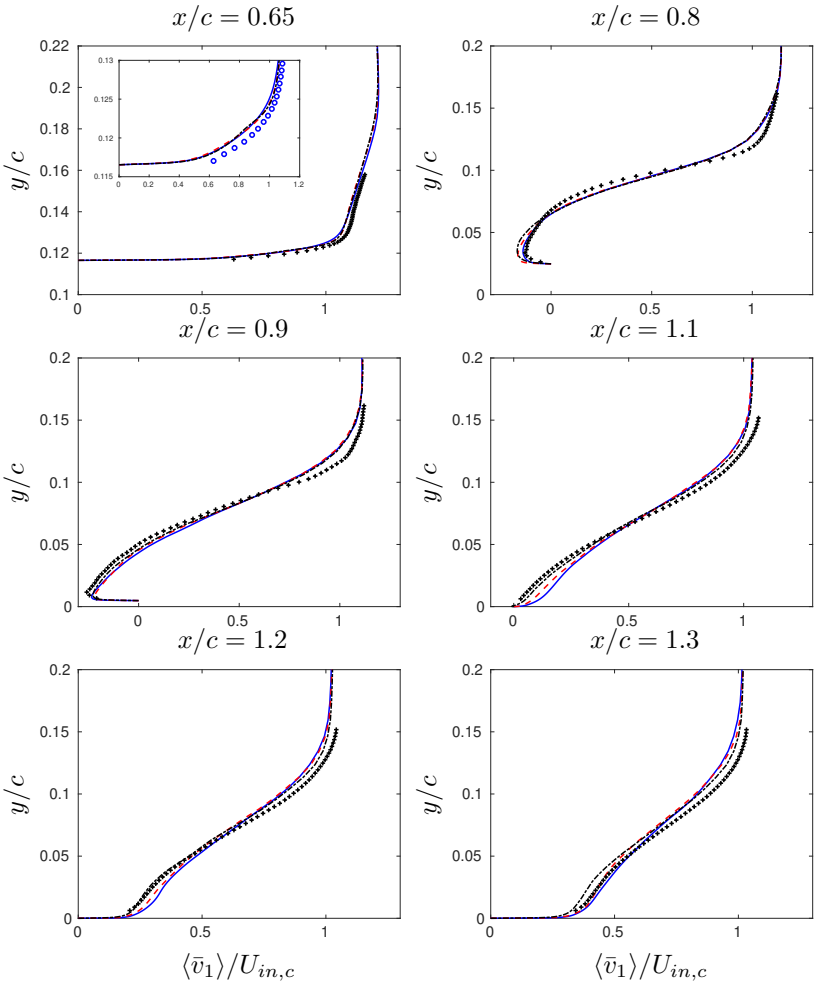

Figure 11: Hump flow. Streamwise velocities. —: D-PANS; – –: IDD-PANS; –·–: IDDES; markers: Experiments [15, 16].

and $f_{k,tar}$ (see e.g. [20] and [9] for discussion). Meanwhile, $f_{k,obs}$ can be obtained from postprocessing, using its definition in Eq. (49).

The comparison is performed upon three test cases: the fully developed channel flow, the hump flow (see Fig. 1), and the hill flow (see Fig. 2).

The comparison is performed regarding various quantities:

- streamwise velocity,
- turbulent kinetic energy and shear stress: total moments, along with their

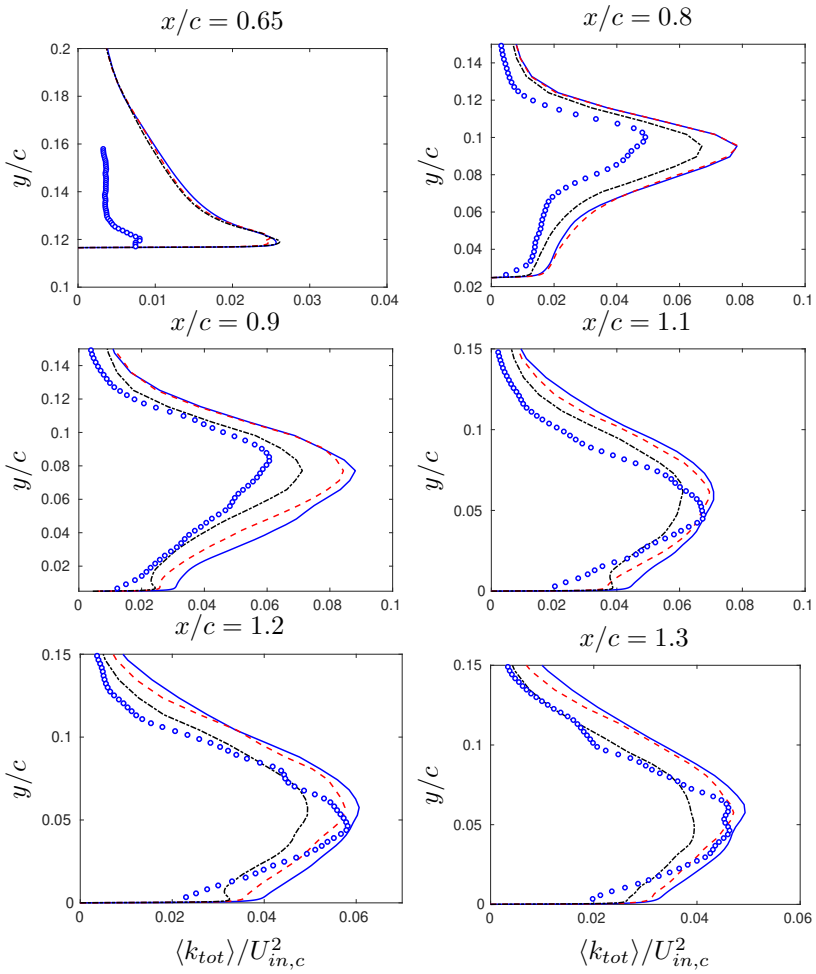

Figure 12: Hump flow. Total turbulent kinetic energy. ——: D-PANS; – – –: IDD-PANS; –·–·–: IDDES; markers: Experiments [15, 16].

repartition between modeled and resolved parts,

- $f_{k,obs}$ and $f_{k,tar}$,

along with case-specific quantities.

4.1. Channel flow

We consider a periodic channel flow at $Re_\tau = u_\tau \delta / \nu = 5\,200$ and $2\ \ 000$, where δ denotes half channel height and u_τ is the friction velocity. The streamwise, wall-normal and spanwise directions are denoted by x, y and z, respec-

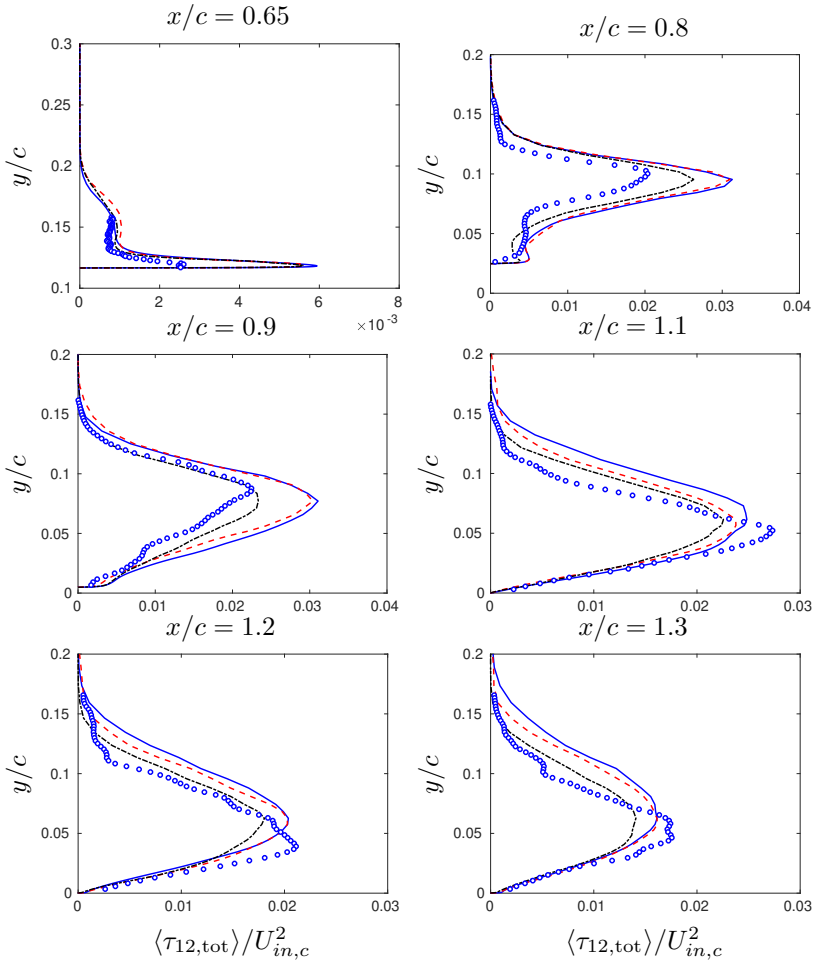

Figure 13: Hump flow. Total turbulent shear stress τ_{12}. ——: D-PANS; – – –: IDD-PANS; —·—: IDDES; markers: Experiments [15, 16].

tively. The size of the domain is $x_{max} = 3.2$, $y_{max} = 2$ and $z_{max} = 1.6$. Two distinct meshes are used (see Table 1). The grid used for the $Re_\tau = 2\,000$ case is a fine, LES-like grid. Periodic boundary conditions are used in the x and z directions. Therefore, these two directions are considered statistically homoge-
225 neous. A precursor DES computation is used as initial condition. The driving pressure gradient (first term on the right hand side in Eq. 48) is used with $\beta = 1$. For the sake of numerical stability, a lower limit of 0.05 is used when computing $f_{k,tar}$ from Eq. (47). Two options on initial conditions, are considered:

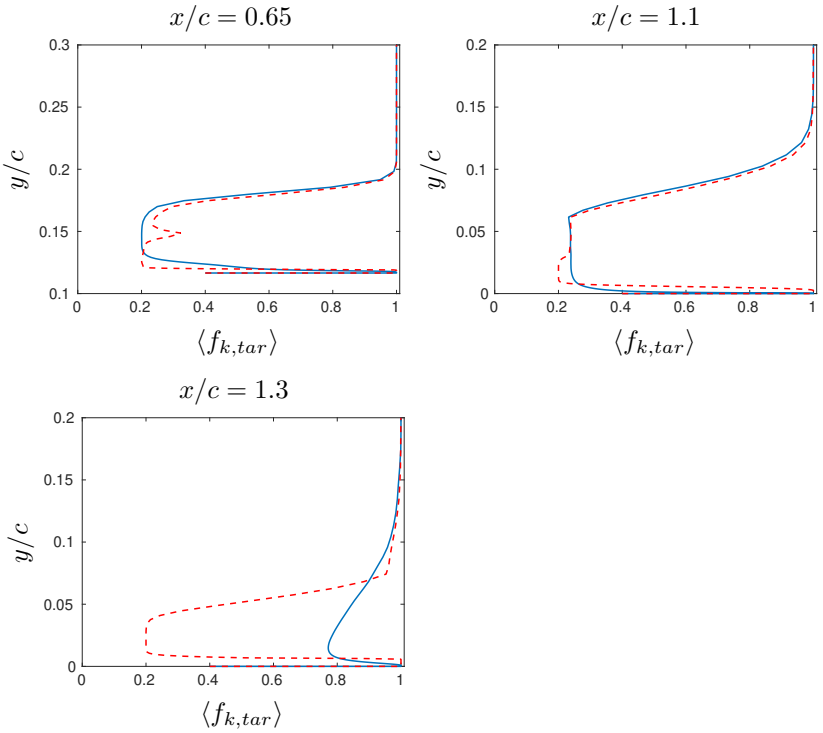

Figure 14: Hump flow. $f_{k,tar}$. ▬: D-PANS; ▬ ▬: IDD-PANS.

Re_τ	$Nx = Nz$	Ny	Δx^+	Δz^+	Δy^+_{wall}	$\Delta y^+_{\text{center}}$
5200	32	96	520	260	0.5	677
2000	64	96	100	50	0.5	213

Table 1: Channel flow: mesh specifications.

- turbulent content (fluctuating),
- no turbulent content (steady),

4.1.1. Fluctuating case

Figure 3(a) presents the mean velocity profile. As can be seen, IDD-PANS is able to match the IDDES profile, and thus performs better than D-PANS. Figures 3(d) shows the ratio between production and dissipation rate of the total turbulent kinetic energy. A small logarithmic zone appears for all three approaches. This is consistent with the total turbulent kinetic energy k_{tot} (Fig. 3b)

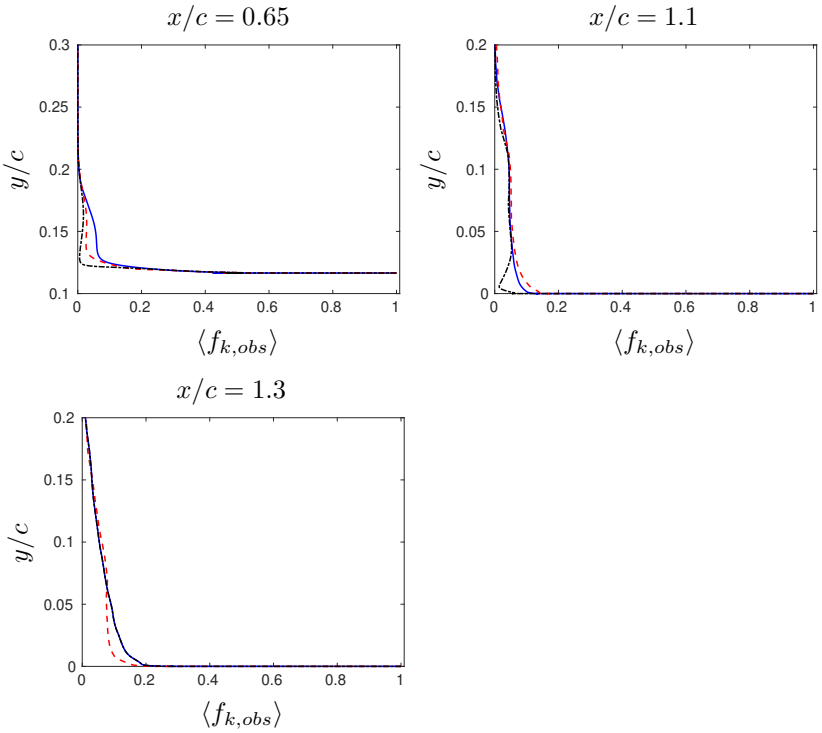

Figure 15: Hump flow. $f_{k,obs}$. ——— : D-PANS; - - - : IDD-PANS; -·-·- : IDDES.

and shear stress $\tau_{12,\mathrm{tot}}$ (Fig. 3c): both quantities exhibit peaks in this logarithmic region of the flow. However, it is worth noticing that the D-PANS k_{tot} profile exhibits a secondary peak. Accordingly, Figs. 4(a) and 4(b), showing respectively modeled and resolved k, show a stronger peak mismatch for D-PANS, than for the other two approaches. For their part, IDD-PANS and IDDES are in good agreement, even with the reference DNS.

Figs. 4(c) and Figs. 4(d) show respectively modeled and resolved parts of the turbulent shear stress τ_{12}. As about k, IDDES and IDD-PANS are in remarkable accordance, while D-PANS differs significantly from the two other approaches. This is consistent with the theoretical background leading to the equivalence criterion between IDD-PANS and IDDES developed in Sec. 2.3; in an equilibrium case like the channel flow, IDD-PANS and IDDES must be equivalent. Eventually, it is also worth noticing that τ_{12} is overall more resolved than k. In other words, if we defined a τ_{12}-equivalent of f_k, called f_{12}, we would

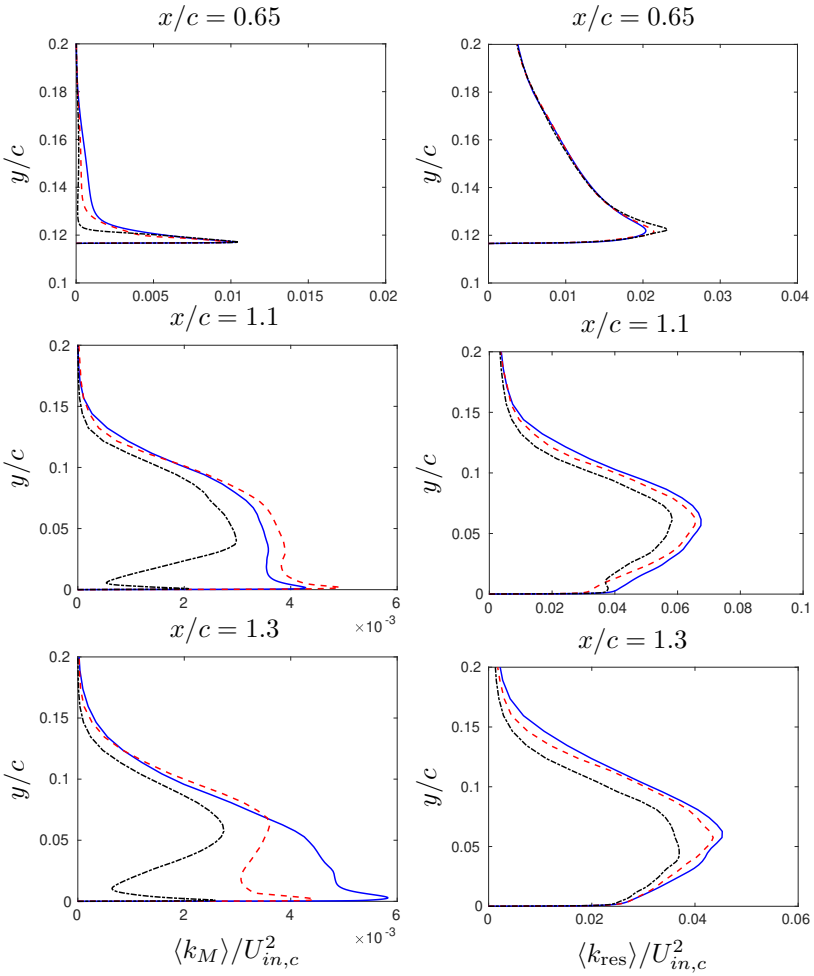

Figure 16: Hump flow. Turbulent kinetic energy: modeled part (left) and resolved part (right). : D-PANS; : IDD-PANS; : IDDES.

have $f_{12} < f_k$, especially toward the center of the channel.

Figure 5(a) compares the target energy ratio $f_{k,tar}$ between D-PANS and IDD-PANS. Note that there is no $f_{k,tar}$ for the IDDES. The shape of the IDD-PANS profile is more complex than D-PANS. This can be explained by the fact
255 that the construction of ψ_{IDDES} is more elaborate than ψ_{DES}, since IDDES is a further evolved version of DES. This complex shape of the IDD-PANS $f_{k,tar}$ profile generates strong wall-normal gradients of $f_{k,tar}$. Interestingly, the lowest plateau of IDD-PANS $f_{k,tar}$, near the wall, corresponds to the area

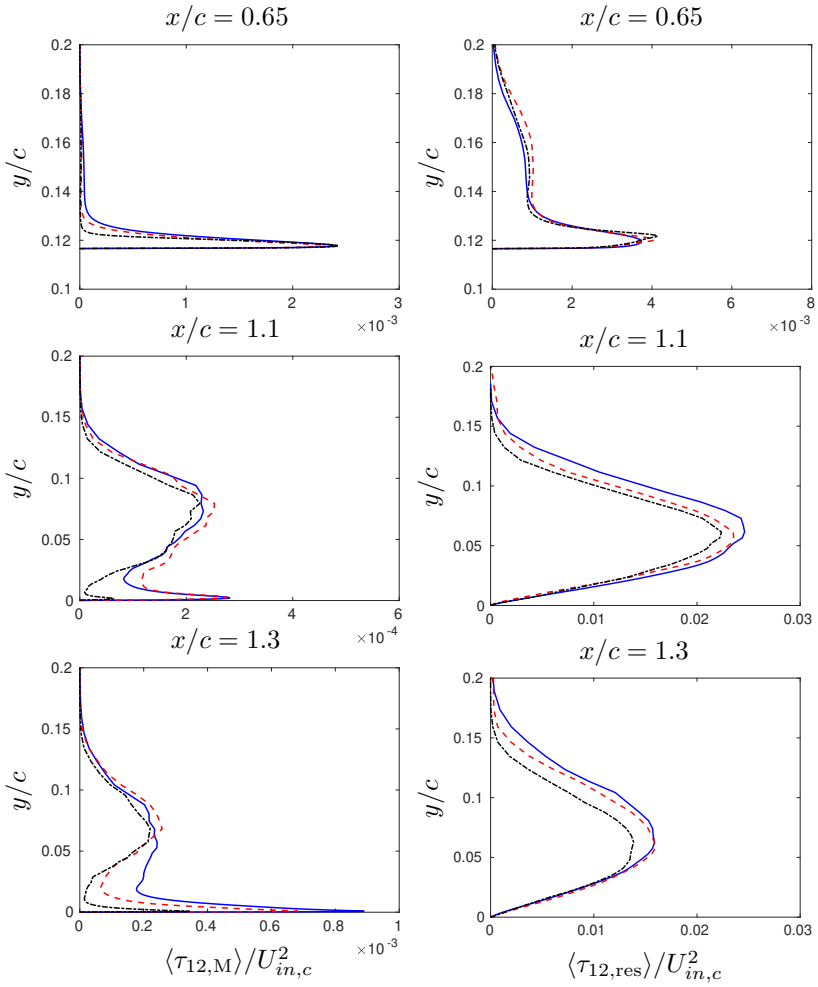

Figure 17: Hump flow. Turbulent shear stress: modeled part (left) and resolved part (right). : D-PANS; : IDD-PANS; : IDDES.

where IDDES differs the most from IDD-PANS. Moreover, the aforementioned sharp wall-normal gradients of $f_{k,tar}$ seem diffused, such that the IDD-PANS $f_{k,obs}$ profile is more regular (see Figure 5b). The latter shows the profiles of the observed energy ratio $f_{k,obs}$ between D-PANS, IDD-PANS and IDDES. As previously with total quantities, one can see that the IDD-PANS profile is very close to that of IDDES, illustrating again that IDD-PANS is able to mimic IDDES, however only approximately.

Figure 6(a) presents the mean velocity profile for the channel case at $Re_\tau =$

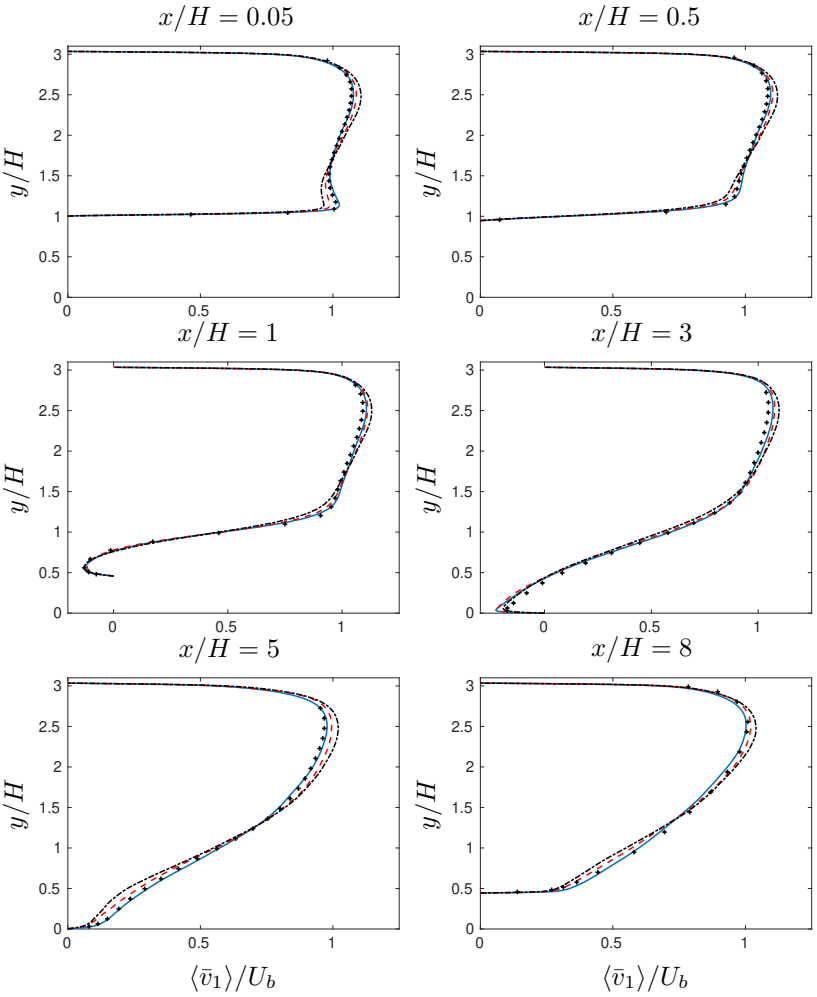

Figure 18: Hill flow. Velocities. —: D-PANS; – –: IDD-PANS; –·–: IDDES; markers: LES [17]

.

2 000. As for the $Re_\tau = 5\,200$ case, IDD-PANS is able to match the IDDES profile, but performs only slightly better than D-PANS. However, IDDES and IDD-PANS do not match the DNS profile at all. This might be due to the fact that one assumption made earlier (all dissipation is contained in the modeled scales) is no longer valid in LES. Accordingly, Figure 6(c) presents similar discrepancies between DNS and the three hybrid approaches, on the total turbulent shear stress profiles. Figure 6(d) shows the ratio between production and

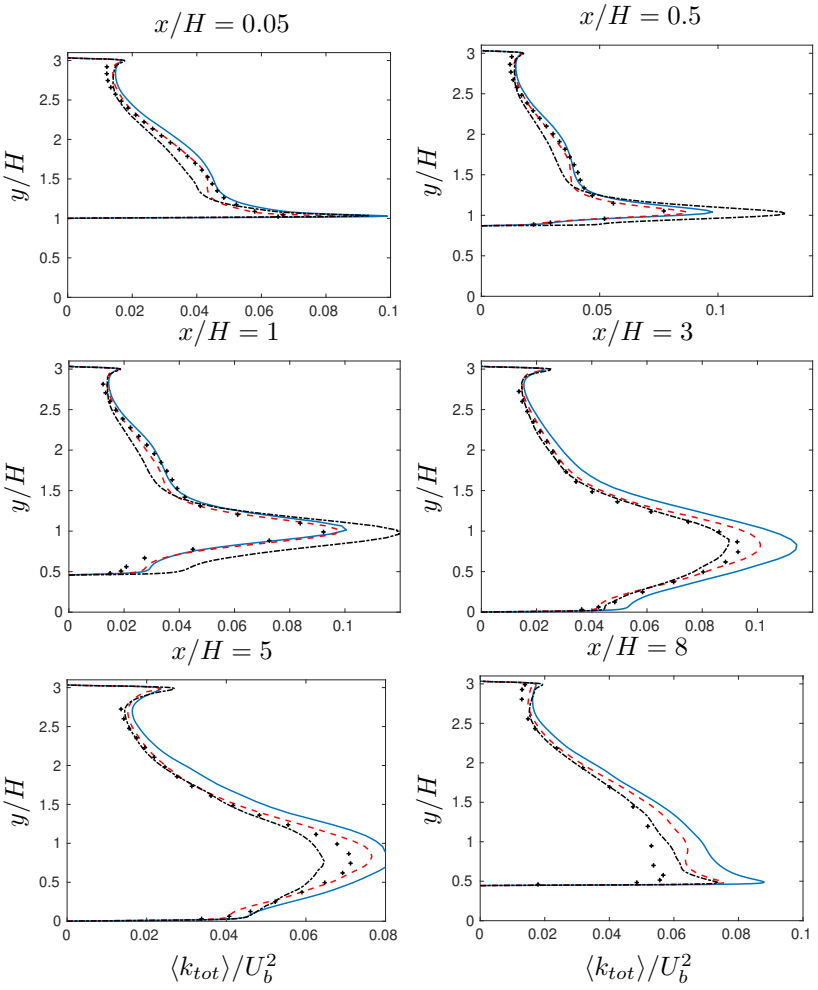

Figure 19: Hill flow. Total turbulent kinetic energy. ——— : D-PANS; – – – : IDD-PANS; –·–·– : IDDES; markers: LES [17]

.

dissipation rate of the total turbulent kinetic energy. A really tiny logarithmic zone appears for all three approaches. This is qualitatively consistent with the fact that Re_τ is lower than previously. Figure 6(b) shows total turbulent kinetic energy profiles. Similarly as previously with the shear stress, IDDES and IDD-PANS are in good mutual accordance, but they differ from the reference DNS, but not as much as D-PANS, particularly in the near-wall region.

Figs. 7(c) and (d) show respectively modeled and resolved parts of the tur-

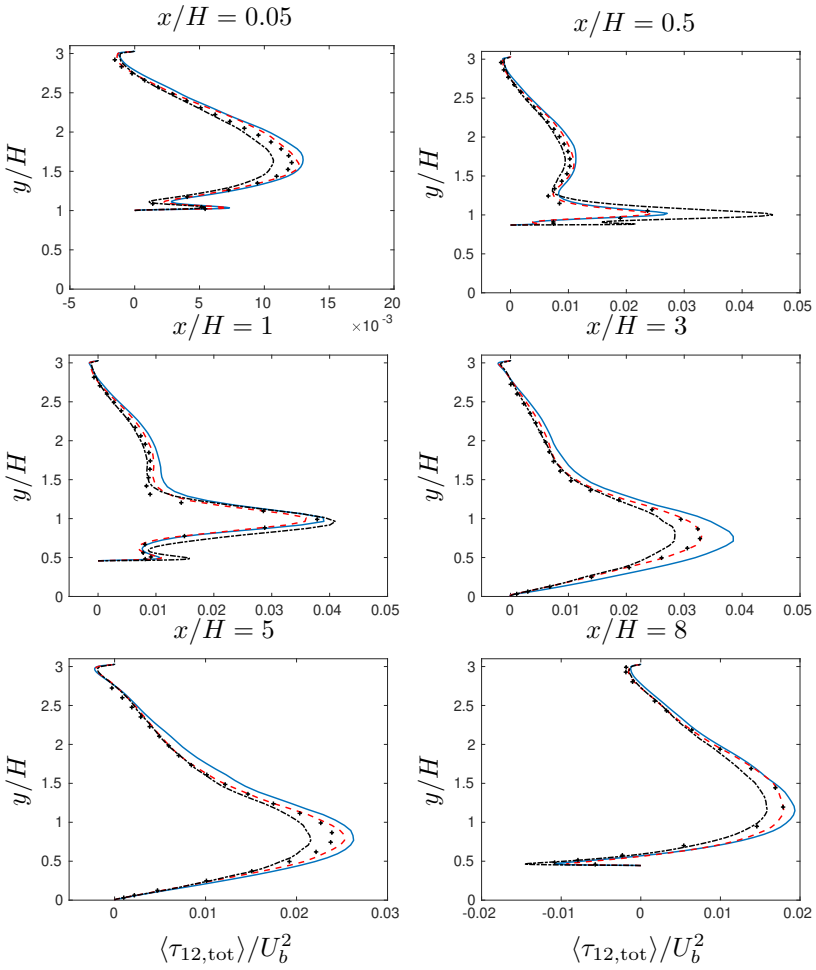

Figure 20: Hill flow. Total turbulent shear stress. — : D-PANS; – – : IDD-PANS; –·– : IDDES; markers: LES [17]

.

bulent shear stress τ_{12}. Figs. 7(a) and (b) show the same repartition, but for the turbulent kinetic energy. As previously with the $Re_\tau = 5\,200$ channel case, the repartition between modeled and resolved scales is remarkably similar between IDD-PANS and IDDES, while D-PANS is clearly different. Moreover,
285 τ_{12} is again overall more resolved than k. In other words, if we defined a τ_{12}-equivalent of f_k, called f_{12}, we would have $f_{12} < f_k$, especially toward the center of the channel.

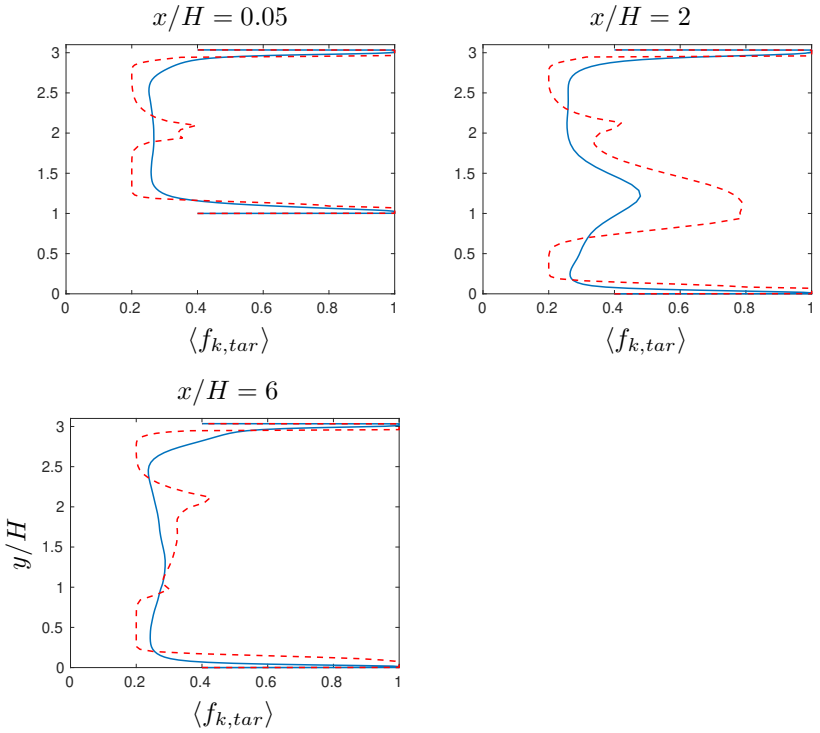

Figure 21: Hill flow. $f_{k,tar}$. ——: D-PANS; – –: IDD-PANS.

Figure 8(a) compares the target energy ratio $f_{k,tar}$ and between D-PANS and IDD-PANS, and Figure 5(b) shows the profiles of the observed energy ratio $f_{k,obs}$ between D-PANS, IDD-PANS and IDDES. It is worth noticing that even though the $f_{k,tar}$ fields are not low enough to perform well-resolved LES in the sense of Pope (less than 20% of the energy must be modeled) in the full channel, the observed energy ratio $f_{k,obs}$ matches the aforementioned criterion, in more than 90% of the channel, for both IDDES and IDD-PANS. Moreover, it seems that D-PANS acts more like a basic hybrid RANS/LES, with a significant modeled part of energy near the wall, while IDD-PANS and IDDES seem to rather adopt the desired behaviour of wall modeled LES. Another interesting fact is that IDD-PANS and D-PANS exhibit similar $f_{k,tar}$ fields toward the middle of the channel, which results in a global accordance in $f_{k,obs}$, also with IDDES. This tendency makes sense at first sight, but it was not observed with $Re_\tau = 5\,200$.

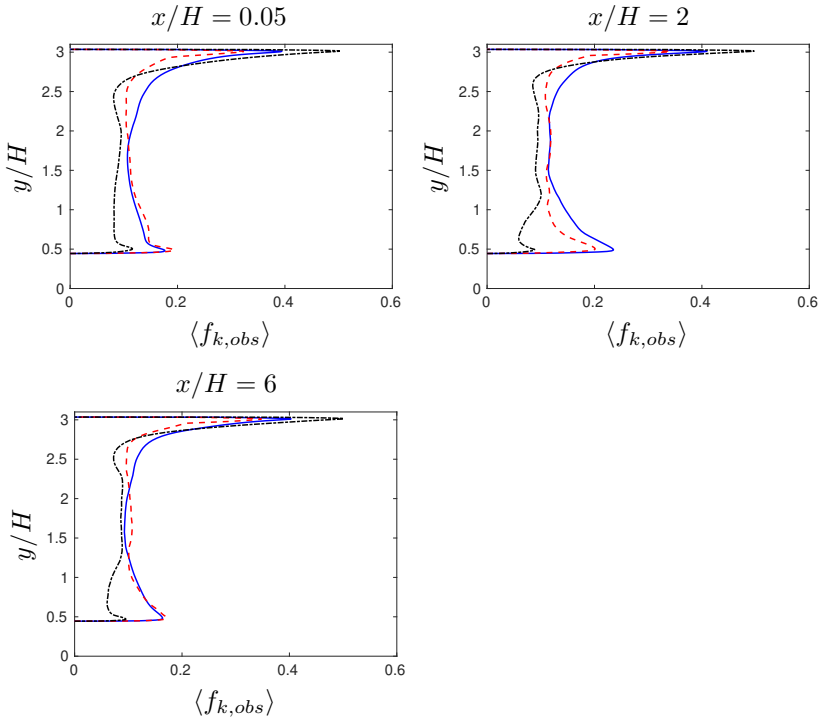

Figure 22: Hill flow. $f_{k,obs}$. ——: D-PANS; – –: IDD-PANS; –·–: IDDES

4.1.2. Steady case

In this case, the initial conditions are fully steady. The friction Reynolds Re_τ is 5 200. Figure 9(a) presents the mean velocity against the DNS results of [14]. There is a good accordance with the DNS reference. Figure 9(b) shows the unresolved eddy viscosity profile, compared with that obtained from a 1D RANS computation, using the same closure model (AKN). The profiles match perfectly, suggesting that in absence of fluctuating initial content, IDD-PANS is able, just like IDDES, to enforce a proper RANS mode. This is confirmed by the fact that IDDES gives $f_{k,tar} = 1$ (not shown).

4.2. Hump flow

The Reynolds number of the hump flow is $Re_c = 936\,000$, based on the hump length, $c = 1$, and the inlet mean velocity at the centerline, $U_{in,c}$. In the present simulations, the values of ρ, c and $U_{in,c}$ have been set to unity.

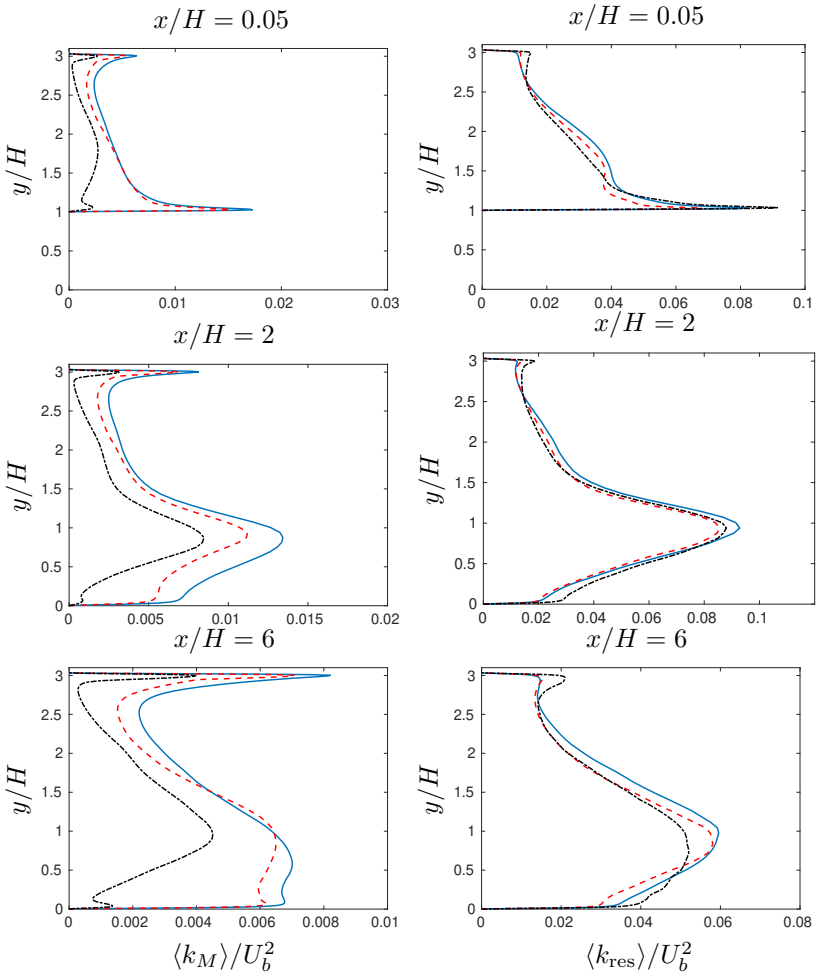

Figure 23: Hill flow. Turbulent kinetic energy: modeled part (left) and resolved part (right). : D-PANS; : IDD-PANS; : IDDES.

The configuration is given in Fig. 1. Experiments were conducted by [15, 16]. The maximum height of the hump, h, and the channel height, H, are given by $h/c = 0.128$ and $H/c = 0.91$, respectively. The mesh has $648 \times 108 \times 64$ cells and is taken from the NASA workshop.[1] The spanwise extent is set to $Z_{max}/c = 0.3$. Initially, a time step of $0.002\ c/U_{in,c}$ was used which worked fine for D-PANS and IDD-PANS; for IDDES, however, the simulation was numerically unstable and

[1] https://turbmodels.larc.nasa.gov/nasahump_val.html

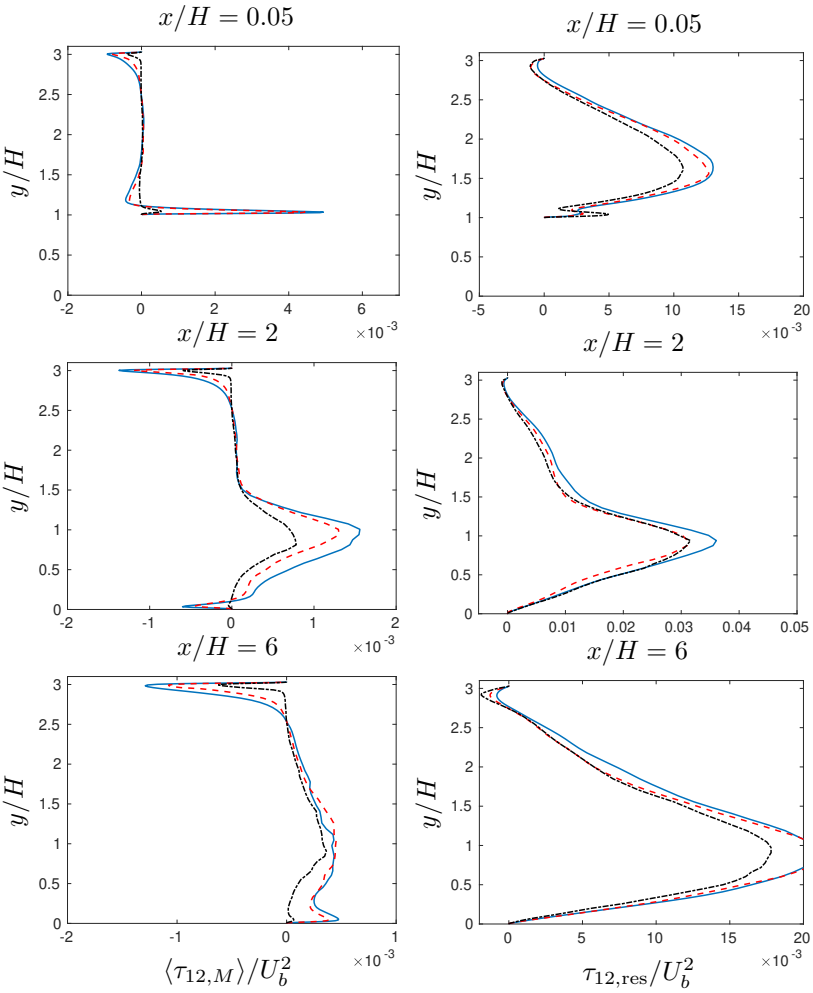

Figure 24: Hill flow. Turbulent shear stress: modeled part (left) and resolved part (right). : D-PANS; : IDD-PANS; : IDDES.

diverged. A smaller time step of 0.001 $c/U_{in,c}$ was chosen for all three turbulence models. The inlet is located at $x/c = -2.1$ and the outlet at $x/c = 4.0$. A periodic boundary condition is applied in the spanwise direction z. Therefore, this direction is considered statistically homogeneous.

325 The conditions (U, V, k and ε) are taken from a 2D RANS simulation with the same momentum thickness as the experimental velocity profiles. The AKN $k-\varepsilon$ turbulence model [11] is used coupled to the EARSM model [21]. Synthetic isotropic fluctuations are superimposed on the 2D RANS velocity field. The

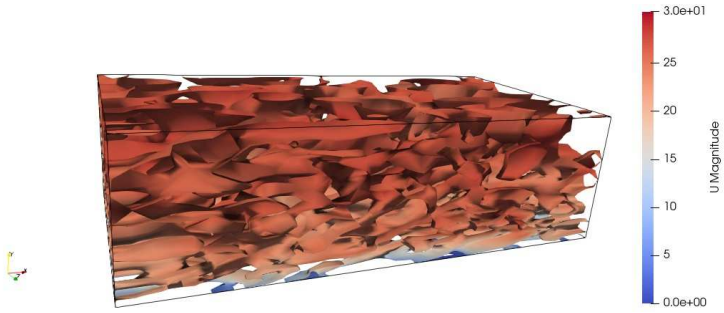

(a) Channel flow, $Q = 10\,(u_\tau/h)^2$

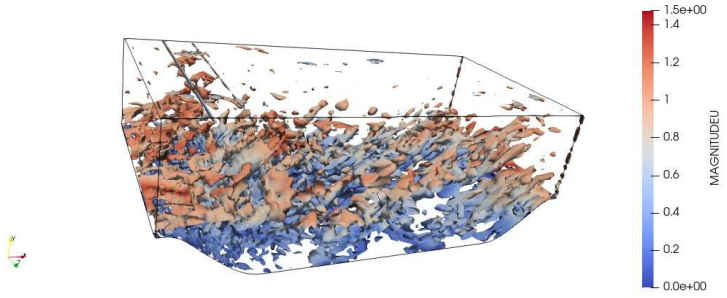

(b) Hill flow, $Q = (U_b/H)^2$

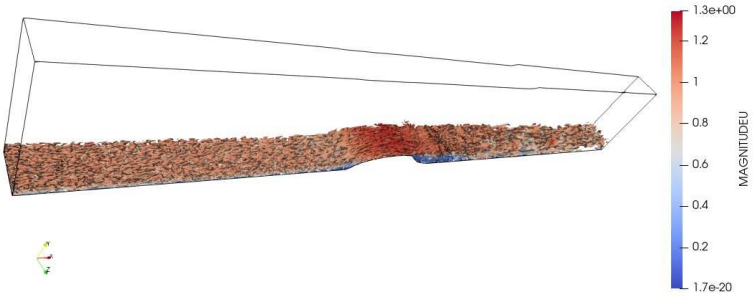

(c) Hump flow, $Q = 3\,(U_{in,c}/c)^2$

Figure 25: IDD-PANS: isocontours of Q-criterion colored by respective instantaneous velocity magnitude.

synthetic fluctuations are scaled with the RANS shear stress profile. To reduce
330 the inlet k, prescribed from 2D RANS, a commutation term $\partial f_k/\partial x$ is used. For more detail on inlet synthetic fluctuations and the commutation term, see [22]. For the sake of numerical stability, a lower limit of 0.2 is used when computing $f_{k,tar}$ from Eq. (47).

The simulations are initialized as follows [23]: first the 2D RANS equations are solved. Anisotropic synthetic fluctuations, $(\mathcal{V}_i')_m$, are then superimposed to the 2D RANS field which gives the initial LES velocity field. In order to compute $(\mathcal{V}_i')_m$, synthetic fluctuations, $v'_{i,synt}$, are computed plane-by-plane $(y-z)$ in the same way as prescribing inlet boundary conditions. The synthetic fluctuations in the $y-z$ planes are coupled with an asymmetric space filter

$$(\mathcal{V}_i')_m = a(\mathcal{V}_i')_{m-1} + b(v'_{synt,i})_m \tag{50}$$

where m denotes the index of the x_1 location and $a = \exp(-\Delta x_1/L_{int})$ and Δx_1 and L_{int} denote the grid size and the integral length scale, respectively $(L_{int} = 0.2)$.

Figure 10(a) compares the profiles of the pressure coefficient C_p. The three models, IDDES, IDD-PANS and D-PANS offer very similar performance, except over the hump at $x/c = 0$, where D-PANS fails in predicting the strong longitudinal gradient of C_p, while IDD-PANS and IDDES succeed. Figure 10(b) shows the skinfriction coefficient C_f profiles. IDDES gives a better agreement with experiment in the boundary layer $(x < 0)$, whereas IDD-PANS shows a better agreement than IDDES and D-PANS in the recirculation region.

Figure 11 shows the streamwise velocity profiles at several locations of the domain, starting from nearly the middle of the hump, to positions located downstream the hump, before and after reattachment. As expected for a flow exhibiting massive separation, the three approaches have a very similar behaviour, except downstream reattachment $(x/c \geq 1.1)$, where IDD-PANS shows some superiority over D-PANS.

Figures 12 (resp. 13) show the total turbulent kinetic energy (resp. shear stress τ_{12}) at the same six locations as above. Before reattachment $(x/c = 0.65, 0.8$ and $0.9)$, all three approaches overestimate $k_{\rm tot}$ and $\tau_{12,\rm tot}$, especially before separation $(x/c = 0.65)$. This might be due to poor resolution of the thin accelerating boundary layer at the upstream part of the hump. One can also notice that there is an overall surprisingly good agreement between IDD-PANS and D-PANS, rather than with IDDES, on those total quantities. They both

capture well the peaks of k_{tot} downstream reattachment, but not those of $\tau_{12,\text{tot}}$, also they do better than IDDES. On the other hand, all three approaches fail at predicting k_{tot} in the near wall region, but perform better on $\tau_{12,\text{tot}}$, especially downstream reattachment ($x/c \geq 1.1$).

Figure 14 compares the targetted values of the energy ratio, $f_{k,tar}$, between IDD-PANS and D-PANS, taken at three locations: slightly before separation ($x/c = 0.65$), and downstream reattachment ($x/H = 1.1$ and $x/H = 1.3$). The shape of the IDD-PANS $f_{k,tar}$ is somewhat more complex than that of D-PANS. Again, this suggests that IDD-PANS inherits the fact that IDDES is more elaborate than DES, as observed for the channel flow. However, the overall values of $f_{k,tar}$ are similar in IDD-PANS and D-PANS, except at $x/c = 1.3$ where the near-wall region is treated nearly in RANS mode by D-PANS ($f_{k,tar} \approx 0.8$), while better resolved by IDD-PANS ($f_{k,tar} \approx 0.2$ at its lowest).

Figure 15 shows profiles of the observed energy ratio, $f_{k,obs}$, compared between IDDES, D-PANS and IDD-PANS, at the same locations as in Fig. 14. Surprisingly, the profiles are very close to each other. The small discrepancies observed, occur in the near wall region. But the most important observation is that, in spite of a moderately resolved input $f_{k,tar}$, the $f_{k,obs}$ are very low, suggesting an overall LES mode. This is caused by the fact that the large resolved scales dominate this out-of-equilibrium flow, as suggested by Figs. 16 (resp. 17). Those latter show the repartitions between modeled and resolved parts of the turbulent kinetic energy (resp. shear stress) at the same three locations. They clearly show that at all of the three locations, the modeled k and τ_{12} are significantly smaller than their resolved counterparts. Accordingly, the latter exhibit a very qualitative agreement, through similar shapes and peak locations, however with various values. In the near wall region and downstream reattachment, the three approaches exhibit significantly different behavior of the modeled quantities, particularly for k_M. This is counterintuitive, since the near wall region is the closest to the RANS mode, thus the three models should behave more similarly, since they share the same parent RANS closure. Finally, before separation ($x/c = 0.65$), one can see that the three approaches agree

quite well, regarding modeled as well as resolved quantities.

4.3. Hill flow

The domain is shown in Fig. 2. The size of the domain is $9H \times 3.035H \times 4.5H$ in the streamwise (x), wall-normal (y) and span-wise direction (z), respectively. The grid has $160 \times 80 \times 32$ cells in the x, y and z direction. Periodic boundary conditions are used in the x and z directions. The z direction is considered statistically homogeneous. Slip conditions are prescribed at the upper wall. The Reynolds number is $Re = 10\,600$ based on the hill height and the bulk velocity U_b at the top of the hill. An initial velocity field is prescribed from a 2D RANS solution with the correct bulk Reynolds number. Furthermore, the same technique for synthetic turbulence as for the hump flow (see Eq. 50), is used to add initial fluctuations. The bulk velocity is then kept constant by adjusting β in Eq. 48 at each time step by ensuring that the sum of the forces at the wall (wall shear stress and pressure on the lower wall) balances the driving pressure gradient [24, 25, Section 4.5].

Figure 18 shows the streamwise velocity profiles at several locations of the domain: on the top of the hill before separation ($x/H = 0.05$ and 0.5), in the expanded area after separation $x/H = 1$, on the bottom of the domain before and after reattachment ($x/H = 3$ and 5), and in the constricted area ($x/H = 8$). As observed in the previous section with the hump flow, the three approaches have a very similar behaviour, except downstream reattachment ($x/H \geq 5$), where IDD-PANS is closer to IDDES than D-PANS.

Figures 19 and 20 show the total turbulent kinetic energy (resp. shear stress τ_{12}) at the six same locations as above. The three hybrid RANS/LES approaches exhibit various behaviors in this flow, but they reasonably capture peaks and inflection points. IDD-PANS seems in overall good agreement with the reference LES of [17], especially regarding $\tau_{12,\mathrm{tot}}$. The performance of IDDES is more debatable, especially upstream reattachment. Surprisingly, D-PANS does not perform as well as the other two approaches on k_{tot}, further downstream separation $x/H \geq 3$, but performs reasonably good on $\tau_{12,\mathrm{tot}}$.

Figure 21 compares the targetted values of the energy ratio, $f_{k,tar}$, between IDD-PANS and D-PANS, at three locations: on the top of the hill ($x/H = 0.05$), in the recirculation bubble ($x/H = 2$) and downstream reattachment ($x/H = 6$). As observed with the other two flows, it is worth noticing that the shape of the IDD-PANS $f_{k,tar}$ profile is slightly more complex than that of D-PANS. Again, this suggests that IDD-PANS inherits the fact that IDDES is more elaborate than DES. However, the overall values of $f_{k,tar}$ are similar in IDD-PANS and D-PANS, except at $x/H = 2$ where the region near $y/H = 1$ is treated nearly in RANS mode by IDD-PANS ($f_{k,tar} \approx 0.8$), while better resolved by D-PANS ($f_{k,tar} \approx 0.45$).

Figure 22 shows profiles of the observed energy ratio, $f_{k,obs}$, compared between IDDES, D-PANS and IDD-PANS, at the same locations as in 21. Interestingly, the $f_{k,obs}$ profiles do not vary much along the domain. The small discrepancies observed are consistent with those observed with modeled k on Fig. 23 and occur mainly close to the walls.

Figures 23 (resp. 24) show repartitions between modeled and resolved parts of the turbulent kinetic energy (resp. shear stress) at the same three locations as above. As for the hump flow, one can notice that at all of the three locations, the modeled k and especially τ_{12} are significantly smaller than their resolved counterparts, which makes sense for a flow exhibiting massive separation, dominated by the large-scale turbulent motion. But contrary to the hump flow, there is no qualitative agreement between the three hybrid RANS/LES approaches, regarding resolved quantities, except on peak and inflection point locations. This is also observed with modeled quantities, however in a less clear way.

Figure 25(a), (b) and (c) show isocontours of the Q-criterion defined by:

$$Q = \frac{1}{2}\left(\bar{\mathbf{S}} : \bar{\mathbf{S}} - \bar{\mathbf{W}} : \bar{\mathbf{W}}\right) \tag{51}$$

with

$$\bar{\mathbf{S}} = \frac{1}{2}\left(\nabla\bar{\mathbf{v}} + \nabla^T\bar{\mathbf{v}}\right) \quad \text{and} \quad \bar{\mathbf{W}} = \frac{1}{2}\left(\nabla\bar{\mathbf{v}} - \nabla^T\bar{\mathbf{v}}\right) \tag{52}$$

Q is normalized by relevant time scales, and colored by the instantaneous

velocity magnitude. Figure 25(a) shows IDD-PANS isocontours of Q for the lower half of the channel flow at $Re_\tau = 5\,200$. Figure 25(b) shows IDD-PANS isocontours of Q for the hill flow, and Figure 25(c) for the hump flow. Quite intuitively, one can observe the finest structures in the hump flow. The hill flow, also dominated by the large-scale motion, which is reasonably resolved, exhibits fine streaks as well. The channel flow, which is the least resolved of the three cases studied here, logically exhibits the coarsest streaks.

5. Concluding remarks

A novel version of PANS, able to behave as IDDES, has been derived theoretically, following the analysis of Friess *et al.* [8] leading to a low-order statistical equivalence they called "H-equivalence". A quantitative relationship has been determined between their respective cutoff functions, namely f_k for PANS and ψ for IDDES, in the framework of stationary and inhomogenous flows, at sufficient high Reynolds number, such that the resolved dissipation rate can be assumed negligible compared to its unresolved counterpart. In the present paper, the analysis is limited to one turbulent closure model, but can be applied to any other.

Though the scale partitioning is less rigorously equivalent than for PITM and DES (see [8]), the main features of IDDES are qualitatively mimicked by the present approach. First, the log-layer mismatch, frequent in attached boundary layer flows, is no longer observed. The IDD-PANS approach gives a better prediction of the mean streamwise velocity than D-PANS, and is very close to the profile predicted by IDDES. Secondly, the approach is able to respond to non-fluctuating inlet or initial conditions, thus able to behave in a proper RANS mode when needed. In particular, the present IDD-PANS approach is able to set the target energy ratio $f_{k,tar}$ to 1 when no turbulent inlet or initial content is provided. However, it is worth noticing that for the hump flow, IDD-PANS turned out to be more stable than IDDES, since the timestep had to be reduced for the latter.

Nevertheless, IDD-PANS does not perfectly match IDDES. The discrepancies between IDDES and IDD-PANS may be due to unadapted assumptions in the derivation of the equivalence criterion. In particular, the assumption that the relative variation of modeled turbulent kinetic $\delta k_M / k_M$ is constant throughout the fluid domain, is very strong and not really suitable for flows where f_k exhibits strong gradients. Moreover, the dissipation rate ε is assumed to be totally modeled (i.e. $f_\varepsilon = 1$), since at high Reynolds numbers, energetic and dissipative scales are sufficiently separated. But (i) near walls, the local Reynolds number is smaller, such that dissipation may occur at resolved scales and (ii) with a sufficiently fine mesh, e.g. in a true LES mode, resolved dissipation must be non negligible. Besides, it is worth noticing that the equivalence between IDDES and IDD-PANS is stronger in the case of the channel flow, than for the two other cases studied here. This can be explained by the fact that the initial "H-equivalence" in [8] was derived for equilibrium flows. The hump and hill flows exhibit massive separation, and thus fall out of this framework.

Further work will focus on calibrating IDD-PANS for other turbulent closures like $k - \omega$, and will be tested with explicit algebraic-like models as well. The effect of accounting for $f_\varepsilon \neq 1$ will be investigated as well.

References

[1] S. S. Girimaji. Partially-averaged Navier-Stokes model for turbulence: A Reynolds-averaged Navier-Stokes to direct numerical simulation bridging method. *ASME Journal of Applied Mechanics*, 73(2):413–421, 2006.

[2] M Klapwijk, T Lloyd, and G Vaz. On the accuracy of partially averaged navier–stokes resolution estimates. *International Journal of Heat and Fluid Flow*, 80:108484, 2019.

[3] B. Chaouat and R. Schiestel. A new partially integrated transport model for subgrid-scale stresses and dissipation rate for turbulent developing flows. *Physics of Fluids*, 17(065106), 2005.

[4] Roland Schiestel and Anne Dejoan. Towards a new partially integrated transport model for coarse grid and unsteady turbulent flow simulations. *Theoretical and Computational Fluid Dynamics*, 18(6):443–468, 2005.

[5] P. R. Spalart, W.-H. Jou, M. Strelets, and S. R. Allmaras. Comments on the feasability of LES for wings and on a hybrid RANS/LES approach. In C. Liu and Z. Liu, editors, *Advances in LES/DNS, First Int. conf. on DNS/LES*, Louisiana Tech University, 1997. Greyden Press.

[6] P. Spalart, S. Deck, M. Shur, K. Squires, M. Strelets, and A. Travin. A new version of detached-eddy simulation, resistant to ambiguous grid densities. *Theoretical and Computational Fluid Dynamics*, 20:181–195, 2006. 10.1007/s00162-006-0015-0.

[7] M. L. Shur, P. R. Spalart, M. Kh. Strelets, and A. K. Travin. A hybrid RANS-LES approach with delayed-DES and wall-modelled LES capabilities. *International Journal of Heat and Fluid Flow*, 29:1638–1649, 2008.

[8] Ch. Friess, R. Manceau, and T.B. Gatski. Toward an equivalence criterion for hybrid RANS/LES methods. *Computers & Fluids*, 122:233–246, 2015.

[9] Lars Davidson and Christophe Friess. A new formulation of f_k for the PANS model. *Journal of Turbulence*, 20(5):322–336, 2019.

[10] J. Ma, S.-H. Peng, L. Davidson, and F. Wang. A low Reynolds number variant of Partially-Averaged Navier-Stokes model for turbulence. *International Journal of Heat and Fluid Flow*, 32(3):652–669, 2011.

[11] K. Abe, T. Kondoh, and Y. Nagano. A new turbulence model for predicting fluid flow and heat transfer in separating and reattaching flows - 1. Flow field calculations. *Int. J. Heat Mass Transfer*, 37(1):139–151, 1994.

[12] M. Gritskevich, A. Garbaruk, J. Schütze, and F. R. Menter. Development of DDES and IDDES formulations for the $k - \omega$ shear stress transport model. *Flow, Turbulence and Combustion*, 88:431–449, 2012.

[13] L. Davidson and C. Friess. The PANS and PITM model: a new formulation of f_k. In *Proceedings of 12th International ERCOFTAC Symposium on Engineering Turbulence Modelling and Measurements (ETMM12), Montpelier, i France 26-28 September*, 2018.

[14] M. Lee and R. D. Moser. Direct numerical simulation of turbulent channel flow up to $Re_\tau \approx 5200$. *Journal of Fluid Mechanics*, 774:395–415, 2015.

[15] D. Greenblatt, K. B. Paschal, C.-S. Yao, J. Harris, N. W. Schaeffler, and A. E. Washburn. A separation control CFD validation test case. Part 1: Baseline & steady suction. AIAA-2004-2220, 2004.

[16] D. Greenblatt, K. B. Paschal, C.-S. Yao, and J. Harris. A separation control CFD validation test case Part 1: Zero efflux oscillatory blowing. AIAA-2005-0485, 2005.

[17] M. Breuer, N. Peller, Ch. Rapp, and M. Manhart. Flow over periodic hills – numerical and experimental study in a wide range of Reynolds numbers. *Computers & Fluids*, 38:433–457, 2009.

[18] Lars Davidson and Shia-Hui Peng. Hybrid LES-RANS: A one-equation SGS model combined with a $k-\omega$ for predicting recirculating flows. *International Journal for Numerical Methods in Fluids*, 43(9):1003–1018, 2003.

[19] P. Emvin. *The Full Multigrid Method Applied to Turbulent Flow in Ventilated Enclosures Using Structured and Unstructured Grids*. PhD thesis, Dept. of Thermo and Fluid Dynamics, Chalmers University of Technology, Göteborg, 1997.

[20] Atabak Fadai-Ghotbi, Christophe Friess, Rémi Manceau, and Jacques Borée. A seamless hybrid rans-les model based on transport equations for the subgrid stresses and elliptic blending. *Physics of Fluids*, 22(5):055104, 2010.

[21] S. Wallin and A. V. Johansson. A new explicit algebraic Reynolds stress model for incompressible and compressible turbulent flows. *Journal of Fluid Mechanics*, 403:89–132, 2000.

[22] L. Davidson. Zonal PANS: evaluation of different treatments of the RANS-LES interface. *Journal of Turbulence*, 17(3):274–307, 2016.

[23] L. Davidson. Non-zonal detached eddy simulation coupled with a steady RANS solver in the wall region. ERCOFTAC Bullentin 89, Special Issue on *Current trends in RANS-based scale-resolving simulation methods*, 2019.

[24] M. Irannezhad. DNS of channel flow with finite difference method on a staggered grid. Msc thesis, Division of Fluid Dynamics, Department of Applied Mechanics, Chalmers University of Technology, Göteborg, Sweden, 2006.

[25] P. Orlandi. *Fluid Flow Phenomena – A Numerical Toolkit*. Kluwer Academic Publishers, 2000.

[26] S. Arvidson, L. Davidson, and S.-H. Peng. Hybrid RANS-LES modeling using a low-Reynolds-number $k-\omega$ based model. In *AIAA Science and Technology Forum and Exposition, AIAA paper 2014-0225, Maryland, 13-17 January*, 2014.

Appendix A. Calculation of the low-Reynolds correction Ψ

Here we detail the derivation of the low Reynolds number correction Ψ entering Eq. (8). To that aim, we follow the methodology explained in [26].

The function Ψ is introduced so that the unresolved eddy viscosity ν_{tu} keeps a Smagorinsky-like shape, even at low Reynolds number, i.e.:

$$\nu_{tu} = C^2 \Delta^2 S \tag{A.1}$$

where $C = \Psi C_{DES}$ is a constant, independent of the ratio ν_{tu}/ν. In other words, the role of Ψ is to de-activate the damping functions.

Let us consider the IDDES system $k_u - \varepsilon_u$ (Eq. (3)) involving the damping functions f_μ and f_2 given by Eq. (2). We define $S^2 = 2\bar{s}_{ij}\bar{s}_{ij}$. In that case, assuming local equilibrium between production and destruction terms in the transport equations for k_u and ε_u respectively yields :

$$\nu_{tu} S^2 = \frac{k_u^{3/2}}{\Psi C_{DES} \Delta} \tag{A.2}$$

$$\nu_{tu} S^2 = \frac{C_{\varepsilon 2}}{C_{\varepsilon 1}} f_2 \varepsilon_u \tag{A.3}$$

The unresolved dissipation ε_u can be eliminated from Eq. (A.3) by linking it to ν_{tu} and k_u :

$$\nu_{tu} = C_\mu f_\mu \frac{{k_u}^2}{\varepsilon_u} \Rightarrow \varepsilon_u = C_\mu f_\mu \frac{{k_u}^2}{\nu_{tu}} \tag{A.4}$$

Putting Eqs. (A.4) and (A.3) together yields:

$$\nu_{tu} S^2 = \frac{C_{\varepsilon 2}}{C_{\varepsilon 1}} f_2 C_\mu f_\mu \frac{{k_u}^2}{\nu_{tu}} \Rightarrow k_u = \nu_{tu} S \sqrt{\frac{C_{\varepsilon 1}}{C_{\varepsilon 2} C_\mu f_\mu f_2}} \tag{A.5}$$

And if we use Eq. (A.5) to express k_u in Eq. (A.2), we obtain:

$$\nu_{tu} = \underbrace{\left(\frac{C_{\varepsilon 2} C_\mu f_\mu f_2}{C_{\varepsilon 1}} \right)^{3/2} \Psi^2 C_{DES}^2}_{C^2} \Delta^2 S \tag{A.6}$$

Now, to make C independant of the damping functions f_μ and f_2, we must have:

$$\Psi^2 = (f_\mu f_2)^{-3/2} \Rightarrow \Psi = (f_\mu f_2)^{-3/4} \tag{A.7}$$

It is worth noticing that this calibration of Ψ is performed only for IDDES, not for IDD-PANS explicitly. Indeed, through Eq. (47), the parameter f_k inherits all (ID)DES features, thus the low Reynolds number correction Ψ.